On the evaluation of strain energy release rate of cement-bone bonded joints under mode II loading

T.D. Campos[1,2], M.L.S. Barbosa[3], M. Martins[4], F.A.M. Pereira[5], M.F.S.F. de Moura[6], Quyền Nguyễn[7], A. Zille[8], N. Dourado[2, 9(*)]

[1] CMEMS-UMINHO, Universidade do Minho, 4800-058, Guimarães, Portugal, teresa.ac.biome@gmail.pt
[2] LABBELS –Associate Laboratory, Braga, Guimarães, Portugal
[3] Faculdade de Engenharia da Universidade do Porto, Portugal, martabarbosa8c@gmail.com
[4] INESC TEC, R. Dr. Roberto Frias, 4200-465 Porto, Portugal, marcos.martins@inesctec.pt
[5] CITAB/UTAD, Departamento de Engenharias, Quinta de Prados, 5001-801 Vila Real, Portugal, famp@utad.pt
[6] Faculdade de Engenharia da Universidade do Porto, Portugal, mfmoura@fe.up.pt
[7] 2C2T-Centro de Ciência e Tecnologia Têxtil, Universidade do Minho, Portugal, quyen@2c2t.uminho.pt
[8] 2C2T-Centro de Ciência e Tecnologia Têxtil, Universidade do Minho, Portugal, azille@det.uminho.pt
[9] CMEMS-UMINHO, Universidade do Minho, 4800-058, Guimarães, Portugal, nunodourado@dem.uminho.pt

Keywords: Cortical bone tissue; Bone fracture; Bone cement; Cohesive Zone Modelling; Finite element model

(*) Corresponding author.
E-mail address: *nunodourado@dem.uminho.pt* (N. Dourado)

Abstract

Bone cements based on poly(methylmethacrylate) (PMMA) are primarily used in joint replacement surgeries. In the fixation of joint replacement, the self-curing cement fills constitutes a very important interface. To understand and improve the interaction between cortical bone and bone cement it is essential to characterize the mechanical properties of cement-bone bonded joints in full detail. In this study, the end-notched flexure test was used in the context of pure mode II fracture characterisation of cement-bone bonded joints. A data reduction scheme based on crack equivalent concept was employed to overcome the difficulties inherent to crack length monitoring during damage propagation. A finite element method combined with a cohesive zone model was first used to validate numerically the adopted method. The procedure was subsequently applied to experimental results to determine the fracture toughness of cement-bone bonded joints under pure mode II loading. The consistency of the obtained results leads to the conclusion that the adopted procedure is adequate to carry out fracture characterisation of these joints under pure mode II loading. The innovative aspect

of the present work lies in the application of cohesive zone modelling approach to PMMA-based cement-bone bonded joints.

Keywords: cement-bone bonded joints, fracture characterisation, mode II loading, cohesive zone modelling.

1. Introduction

Cortical bone tissue and skeleton joints of the human body show a remarkable mechanical performance in many daily life activities. However, on many occasions they are exposed to adverse actions that can lead to damage (e.g., fracture) or to long-term efforts that can cause severe arthritis. These serious conditions reduce the ability of the human body to move, decrease quality of life in many ways, and entail major costs for national health services. Over the years, several techniques have been developed aiming the appropriate healing of bone tissue, in the case of bone fractures, and the repair of skeleton joints, by fitting prosthetic devices. Considerable advances were made over the years through the employment of numerous materials exhibiting biocompatibility and stability features that emerged originally in other areas of engineering. This was possible mainly because the mechanical behaviour of those materials was already well known, thus offering a basis of trust that was required for those means. New requirements motivated by rejection episodes that have come to light mainly among the elderly population and the also the need to produce an increasing number of customized solutions for injured people, impel researchers and engineers throughout the world to develop solutions to allow the fixation of prosthetic devices or produce new bone-fracture repairing systems. Such an effort however requires further development of more effective fixation methods for biomedical devices that may involve the employment of bone cements. Therefore, it is vital to know the mechanical behaviour of bond-bone tissue interfaces in more

detail, namely their fracture toughness under different loading modes. The evaluation of bone toughness and fracture mechanisms arise thus as crucial research topics to improve many existing biomedical fixation devices (as protheses).

Fracture studies found in the literature are predominantly dedicated to mode I fracture. However, a considerable number of fractures in bone are induced by shear loading, which occur during torsion and twisting efforts in many daily life activities. Predictions of fracture growth, as well as stress and displacement fields are possible to obtain, by combining the Finite Element Method (FEM) with Cohesive Zone Models (CZM), providing that suitable failure criteria are used. In fact, CZM are particularly adequate to deal with quasi-brittle materials characterized by the existence of a non-negligible fracture process zone, such as cortical bone tissue [1]. de Moura et al. [2] performed a numerical analysis on the application of the ELS and ENF tests to undergo pure mode II fracture characterisation of bone. The main concerns of their study were related to specimen dimensions available in bone versus extensive fracture process zone that develops under pure mode II loading. Effectively, it must be guaranteed that self-similar crack growth occurs for a given crack extent in order to provide a valuable measurement of fracture energy. Dourado et al. [1] studied the adequacy of the ENF test to accomplish mode II fracture characterisation of young bovine cortical bone. Furthermore, a compliance-based beam method (CBBM) was pursued due to difficulties intrinsic to crack monitoring during its propagation. A trapezoidal cohesive zone law was used to validate numerically the proposed approach. The authors concluded that the ENF, the data reduction method and the cohesive law estimation both propitiate straightforward and appropriate procedures to perform fracture characterisation of bone under pure mode II loading.

Bone-shaft fracture repair requires proper alignment during the recovery phase to ensure correct healing. When external fixation procedures (e.g., plaster systems) are not adequate to ensure bone alignment, it becomes necessary to apply internal fixators devices. However, conventional

internal fixation procedures are associated with several clinical problems [3]. As such, the development of other stabilisation systems, ideally non-metallic and in the form of adhesives, could be a colossal asset to improve bone fracture repair.

Bone cement has been used in the fixation of implants in orthopaedic and traumatic surgeries, to act as a load distributor domain between the artificial implant and bone wall. Polymethylmethacrylate (PMMA) is the main constituent of the most widely used bone cement nowadays, due to its biostability and good mechanical properties [4-6]. Debonding, cracking of cement mantle, and loosening of cemented hip arthroplasties can originate serious complications requiring revision surgery [7]. In this context, the study of the bone-cement bonded joints, subjected to different types of loads, considering bone as the substrate becomes relevant. The debonding of implant-cement interfaces induce the failure of cemented femoral prostheses by shear loading [8], so it is important to study the shear strength. Some test methods are known to determine fracture properties, such as fracture toughness and impact strength. Bone cement is considered a linear elastic material, given the brittle behaviour of PMMA, allowing an easy determination of fracture properties [9]. Therefore, the fracture toughness of PMMA bone cements has been studied over the years [10]. Mann et al. [11] are also dedicated to the study of the mechanical behaviour of the cement-bone interface. The authors concluded that mechanical fracture tests yield good results, valid for application to constitutive models of the cement-bone interface within a finite element context. In fact, a work by the same authors points out that the inclusion of test results with shear loading for pure mode II in constitutive models correctly recreates the structural response of experimental specimens [12].

Therefore, to understand and preview the interaction between bone and bone cement it is essential to characterize the mechanical properties of bone-cement bonded joints in full detail. The objective of this study is to determine the mechanical behaviour of the cement-bone bonded joints due to pure mode II loading. The good results of the procedures adopted in the

characterisation of bone fractures under pure mode II loading using the ENF test [1] encouraged the authors to employ a strategy similar to bone-cement bonded joints. Therefore, in this study bone-cement bonded joints were manufactured with ENF configuration for quasi-static pure mode II fracture characterisation. *Resistance*-curves (*R*-curves) were evaluated using the compliance-based beam method (CBBM). An inverse method was adopted combining the Finite Element Method and experimental data to identify cohesive laws, which allows mimicking damage initiation and propagation in the adhesive layer. The developed procedure rendered possible to determine the critical strain energy release rate of bone-cement bonded joint.

2. Experiments

2.1 Preparation of biological samples

Four bovine femurs from adult animals were selected to obtain specimens of cortical bone tissue from the internal medial region of the diaphysis (Fig. 1). Bone shafts were split in two halves with a ceramic disk (0.8 mm thick; BUEHLER® ref. 111190) and then milled (16 mm diameter end mill, from Sandvik Coromant® ref. R216.34-16050) to obtain parallelepiped samples of similar sizes. Bone samples were wrapped in gauzes suitably moistened with saline solution to keep the osmotic equilibrium and then frozen at -20°C.

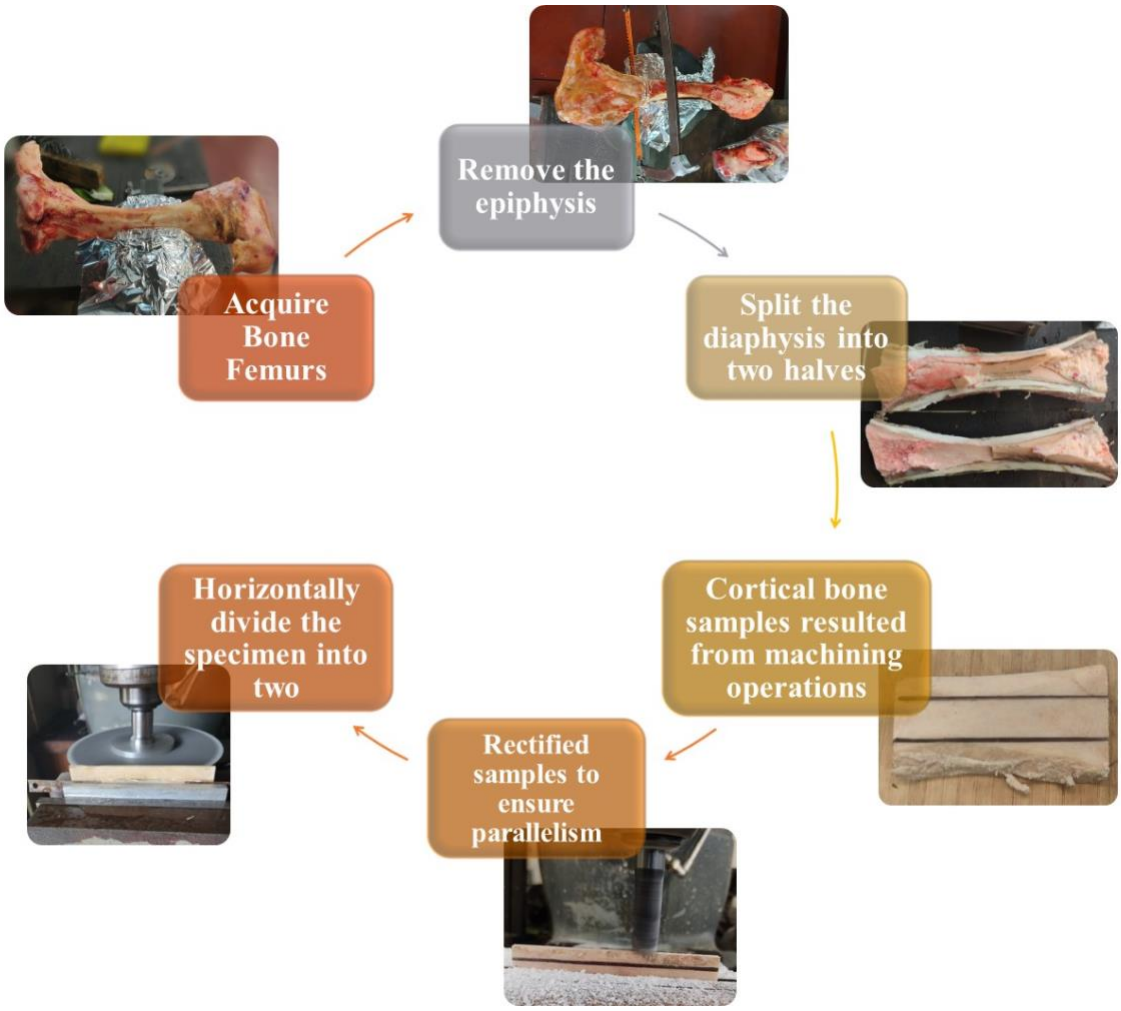

Fig. 1 Manufacturing phases of specimens of cortical bone tissue.

2.2 Preparation of bone cement

Used Polymethylmethacrylate (PMMA) cement (DePuy® Synthes | J&J Company ref. CMW 3) consists of a powder base and a liquid monomer (Fig.2). Bone cement was prepared according to DePuy® datasheet instructions. To prevent the formation of pores, the components were mixed homogeneously, thus obtaining a mass with proper viscosity.

Fig. 2 Bone-Cement production process.

2.3 Preparation of bonded joints

Bonded joints were prepared by first smearing one of the bone arms with bone-cement and then joined firmly onto the other arm, while keeping the parts under pressure for 24 hours (Fig. 3). This operation was preceded by gluing an adhesive tape at the crack tip to define the initial crack length a_0. In addition, cement joint thickness was ensured by insertion of a Teflon® foil (thickness 0.2 mm) between both specimen arms prior to the application of pressure. Specimens were kept in room conditions (25°C and 65% RH) in the course of the bonding operations.

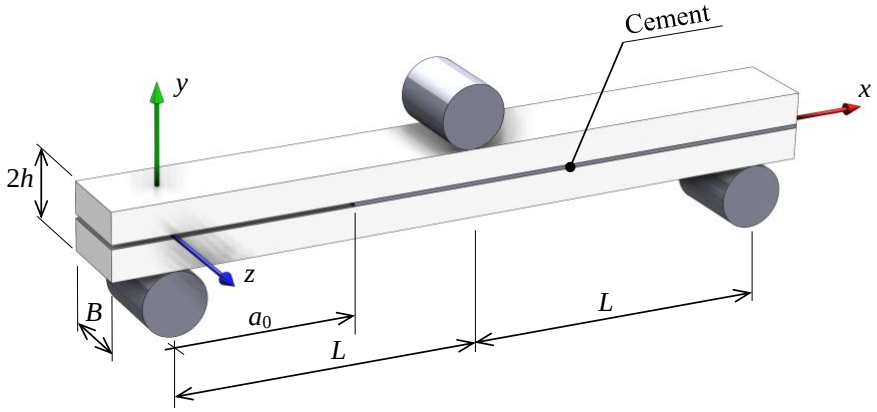

Fig. 3 Cement-bone bonded joint for an ENF test.

Table 1 presents the dimensions of cement-bone bonded joints (Fig. 3), together with the initial crack length (a_0) for the ENF tests.

Table 1: Specimen dimensions (in mm)

Specimen	a_0	$2h$	B	$2L$
1	23.1	7.6	9.1	90
2	21.9	7.8	9.7	100
3	21.9	10	7.8	100
4	22.7	8.2	9.4	90

2.4 Mechanical tests

The end-notched flexure (ENF) test was chosen for fracture characterisation of the cortical bone-cement bonded joint under pure mode II loading (Fig. 4). An Instron® 8801 testing system was used with a load-cell of 5 kN at room temperature (25°C; 65% RH). The loading rate was regulated to 3 mm/min, with an acquisition frequency set to 5 Hz. Two foils of Teflon® with a fine oil-pellicle were inserted in the pre-crack region to reduce friction due to relative movements during the test. Load-displacement values were recorded in the course of the loading process until final rupture.

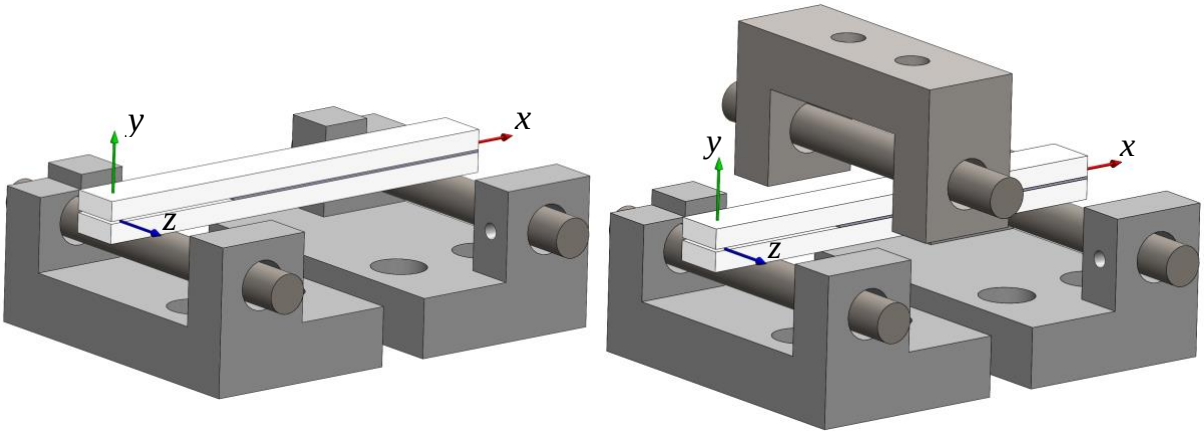

(a) (b)

Fig. 4 Schematic representation of the ENF test on cement-bone bonded specimen: (a) simply supported (prior to test) and (b) fully-assembled.

3. Compliance-based beam method

This method allows measuring the strain energy release rate under mode II loading G_{II} as a function of the crack length a, employing uniquely the P-δ curve obtained experimentally. The required data is the current compliance $\left(C=\delta/P\right)$, which can be equated to both dimensional (Fig. 3) and elastic parameters, considering the Timoshenko beam theory [1],

$$C=\frac{3a^3+2L^3}{8Bh^3E_{\mathrm{L}}}+\frac{3L}{10BhG_{\mathrm{LR}}} \tag{1}$$

where L stands for the mid-loading span, B for the specimen width, h for the mid-height, and E_{L} and G_{LR} for the elastic longitudinal and shear moduli, respectively. To account for the scatter of elastic properties, as well as for stress concentrations at the crack tip, the elastic modulus E_{L} was estimated numerically (FEM) by fitting the initial stiffness with a crack length equal to a_0. Owing to its minor influence of the results, a typical value of G_{LR} can be used in this fitting procedure.

Hence, solving Eq. (1) to the crack length (hereafter referred to as the equivalent crack length), turns

$$a_{\mathrm{e}}=\left[\frac{C_{\mathrm{c}}}{C_{0\mathrm{c}}}a_0^3+\frac{2}{3}\left(\frac{C_{\mathrm{c}}}{C_{0\mathrm{c}}}-1\right)L^3\right]^{\frac{1}{3}} \tag{2}$$

where,

$$C_{\mathrm{c}}=C-\frac{3L}{10BhG_{\mathrm{LR}}};\quad C_{0\mathrm{c}}=C_0-\frac{3L}{10BhG_{\mathrm{LR}}} \tag{3}$$

Combining the Irwin-Kies equation,

$$G_{\mathrm{II}}=\frac{P^2}{2B}\frac{dC}{da} \tag{4}$$

with Eq. (1), the mode II energy release rate is obtained as a function of the equivalent crack length [1],

$$G_{\mathrm{II}}=\frac{9P^2a_{\mathrm{e}}^2}{16B^2h^3E_{\mathrm{L}}} \tag{5}$$

4. Cohesive zone model

The stepwise cohesive zone law (Fig. 5) [13] was used to simulate damage initiation and propagation in bone-cement joints. A constitutive relationship between the shear traction (σ_{II}) and relative displacements (δ_{II}) was established.

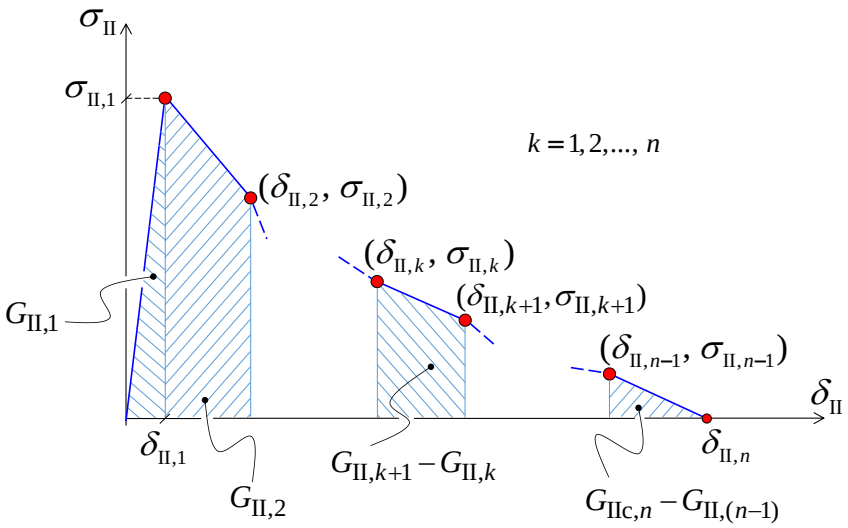

Fig. 5 Stepwise cohesive law ($G_{\mathrm{IIc}}=\sum_{k=1}^{n}G_{\mathrm{II},k}$).

In the initial linear branch, the shear tractions (σ_{II}) are related with the relative displacements (δ_{II}) as follows,

$$\sigma_{\mathrm{II}} = K\delta_{\mathrm{II}} \tag{6}$$

with *K* chosen by the user to express the shear interface stiffness. This parameter should be sufficiently high (within the range $1E6 \le K \le 1E7$ N/mm^3) to avoid compromising the specimen compliance and prevent numerical instabilities. Following damage initiation (i.e., $\delta_{\mathrm{II}} \ge \delta_{\mathrm{II},1}$), the constitutive law (Eq. 6) is modified according to,

$$\sigma_{\mathrm{II}} = (1-d)K\delta_{\mathrm{II}} \tag{7}$$

where *d* represents the damage parameter, which varies within the interval [0, 1]. The relative displacement δ_{II} and tractions σ_{II} at the transition points ($k = 2,3,,...,n$) (Fig. 5) are used to represent the cohesive law. The combination of Eq. (7) with the corresponding softening relation,

$$\sigma_{\mathrm{II}} = \frac{\sigma_{\mathrm{II},k} - \sigma_{\mathrm{II},(k-1)}}{\delta_{\mathrm{II},k} - \delta_{\mathrm{II},(k-1)}}\left(\delta_{\mathrm{II}} - \delta_{\mathrm{II},(k-1)}\right) + \sigma_{\mathrm{II},(k-1)} \text{ for } \delta_{\mathrm{II},(k-1)} \le \delta_{\mathrm{II}} \le \delta_{\mathrm{II},k} \tag{8}$$

allows determining the damage parameter *d* for each segment. Therefore, the evolution of parameter *d* is accomplished differently in successive stages (branches), as follows

$$d = 1 - \frac{1}{K\delta_{\mathrm{II}}}\left[\frac{\sigma_{\mathrm{II},k}\left(\delta_{\mathrm{II}} - \delta_{\mathrm{II},(k-1)}\right) + \sigma_{\mathrm{II},(k-1)}\left(\delta_{\mathrm{II},k} - \delta_{\mathrm{II}}\right)}{\delta_{\mathrm{II},k} - \delta_{\mathrm{II},(k-1)}}\right] \text{ for } \delta_{\mathrm{II},(k-1)} \le \delta_{\mathrm{II}} \le \delta_{\mathrm{II},k} \tag{9}$$

The ultimate relative displacement $\delta_{\mathrm{II},n}$ derives from the mode II critical strain energy release rate,

$$G_{\mathrm{IIc}} = \sum_{k=1}^{n} \frac{(\sigma_{\mathrm{II},k} + \sigma_{\mathrm{II},(k-1)})(\delta_{\mathrm{II},k} - \delta_{\mathrm{II},(k-1)})}{2} \tag{10}$$

which corresponds to the total area of the softening law (Fig. 5).

5. Numerical analysis

Two-dimensional plane-stress analyses were conducted considering a finite element mesh formed by 810 solid quadrilateral finite elements (with 8-nodes) and 90 compatible cohesive finite elements with null thickness (6-nodes). These elements were distributed along the specimen half-eight to simulate damage initiation and propagation along the bonding line (Fig. 6). Open cohesive elements (shear stress-free transfer but transmitting compressive normal stresses when contact arises) disposed along the initial crack allowed to mimic the initial crack length occupied by the Teflon® foil in the experiments. The mesh was refined in the region of crack initiation and propagation to allow stable damage development and growth during loading. Boundary conditions were suitably defined to simulate the supports (simply support) and the prescribed loading displacement at the specimen mid-span. Fracture was induced through a vertical displacement applied at the mid-span. Loading displacement with small increments (0.01% of total applied displacement) was considered to assure smooth damage propagation.

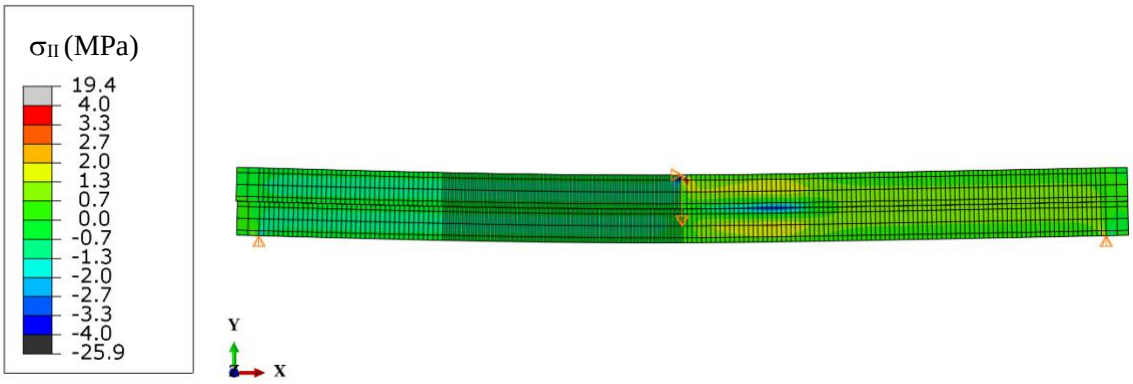

Fig 5 Shear stress cartography in the ENF test.

Due to negligible thickness of the cement layer, the used cohesive elements were programmed with null thickness, by means of a developed user-subroutine. Cortical bone tissue was

considered a transversally isotropic homogeneous material, with linear elastic behaviour (Table 2).

Table 2 Elastic properties of bovine cortical bone [14]

E_L (MPa)	E_T (GPa)	G_{LT} (GPa)	ν_{LT}
*	9.55	4.74	0.37

* By numerical agreement for each specimen to reproduce the experimental initial stiffness.

5.1 Inverse method

The identification of the cohesive law (CL) of bonded joints was accomplished by means of an inverse method (Fig. 7) that combines numerical and experimental data to obtain the agreement of the ensued load-displacement curves ($P-\delta$ curves). The methodology requires the experimental load-displacement curve for each specimen *j*, from which both the elastic modulus E_L and the critical strain energy release rate (i.e., the horizontal asymptote of the *Resistance*-curve) G_{IIc} are determined from the CBBM (Eqs. (1), (2) and (5)). Then, the cohesive law (Fig. 5) is estimated by first considering a cohesive strength (iteration *k*) $\sigma_{II,k}$ with Eqs. (6) and (7), and the corresponding finite element analysis (Fig. 6) performed by assuming the elastic properties of cortical bone tissue (Table 2). The ensued $P-\delta$ curve is then compared with the experimental one, considering the objective function

$$Dif_k = 0.5\sum_{i=1}^{m}(P_i^{n} - P_i^{e}) \tag{11}$$

where P_i^{n} and P_i^{e} represent respectively the numerical and experimental load, took from the set of points forming the $P-\delta$ curve excluding the linear domain. The solution is then found recursively, when a minimum value is attained for the quantity Dif_k.

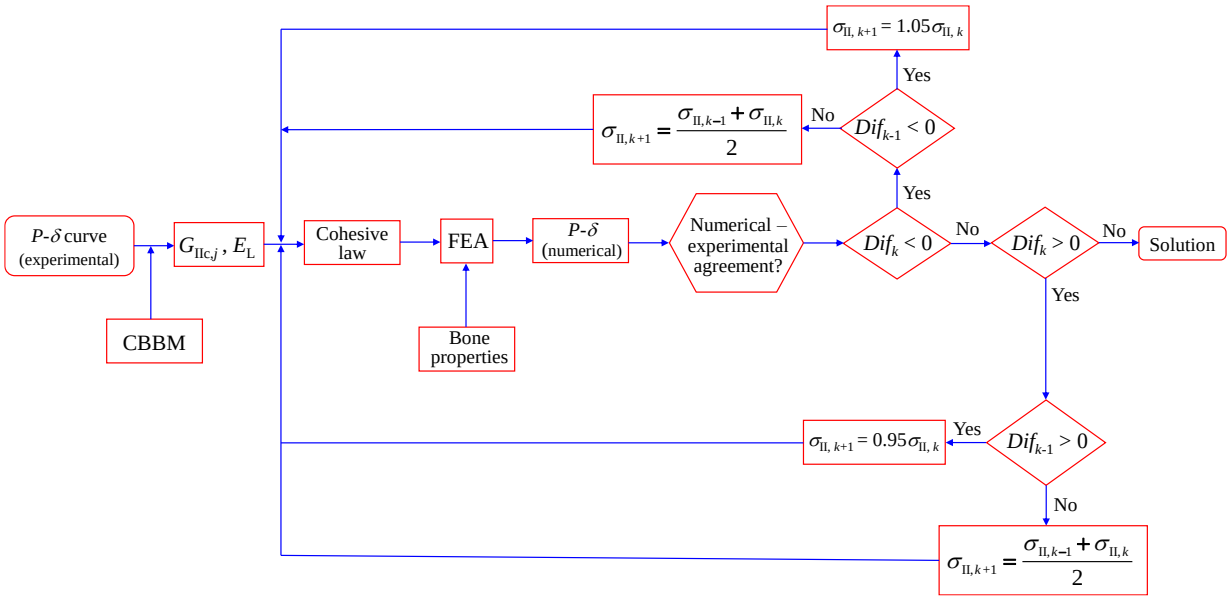

Fig 7 Flowchart showing the applied methodology to obtain cohesive parameters.

5.2 Cohesive Zone Modelling

One of the crucial features of the suggested inverse method is the development of a suitable CZM process appropriate for bone fracture simulation under mode II loading. According to this numerical procedure, when the shear relative displacement exceeds its linear-elastic limit $\delta_{II,1}$, irreversible damage develops reflecting on a non-linear region of the $P-\delta$ curve (Fig. 8) ahead of the crack tip. Initially, as the displacement increases, the cohesive element adjacent to the crack tip quickly achieves its maximum interfacial shear traction ($\sigma_{II,u}$) and undergoes a relative displacement in the softening zone (i.e., in the descending branch of the cohesive law, Fig. 5). Further energy applied to the system allows developing the cohesive zone till its critical size (l_{CohC}), which should correspond to the release of fracture energy under self-similar condition. At this stage, the accurate measurement of the critical strain energy release rate under mode II loading (G_{IIc}) is achieved. In the ENF test, the development of the cohesive zone tends to be influenced by the compressive stresses developing in the vicinity of the (loading) actuator, which spuriously increase the energy release rate due to the rise of energy at the crack tip. Due to this disturbance, in such cases the value of G_{IIc} is not attained. Consequently, the need to

properly design the ENF experimental test is perceptible, which can be performed combining numerical and experimental data.

6. Results and discussion

The ENF test was applied to estimate the strain energy release rate of bone-cement bonded joints under pure mode II loading by means of the *Resistance*-curve (*R*-curve). For test monitoring (just qualitatively), four black lines were marked on the specimen ahead of the crack tip (Fig. 9) prior to fracture tests (from top to bottom). In the course of the loading process, those lines were visibly misaligned due to relative displacement along the bonding plane due to damage propagation under mode II loading. Joint debonding was clearly observed following the load drop and unloading (Fig. 9).

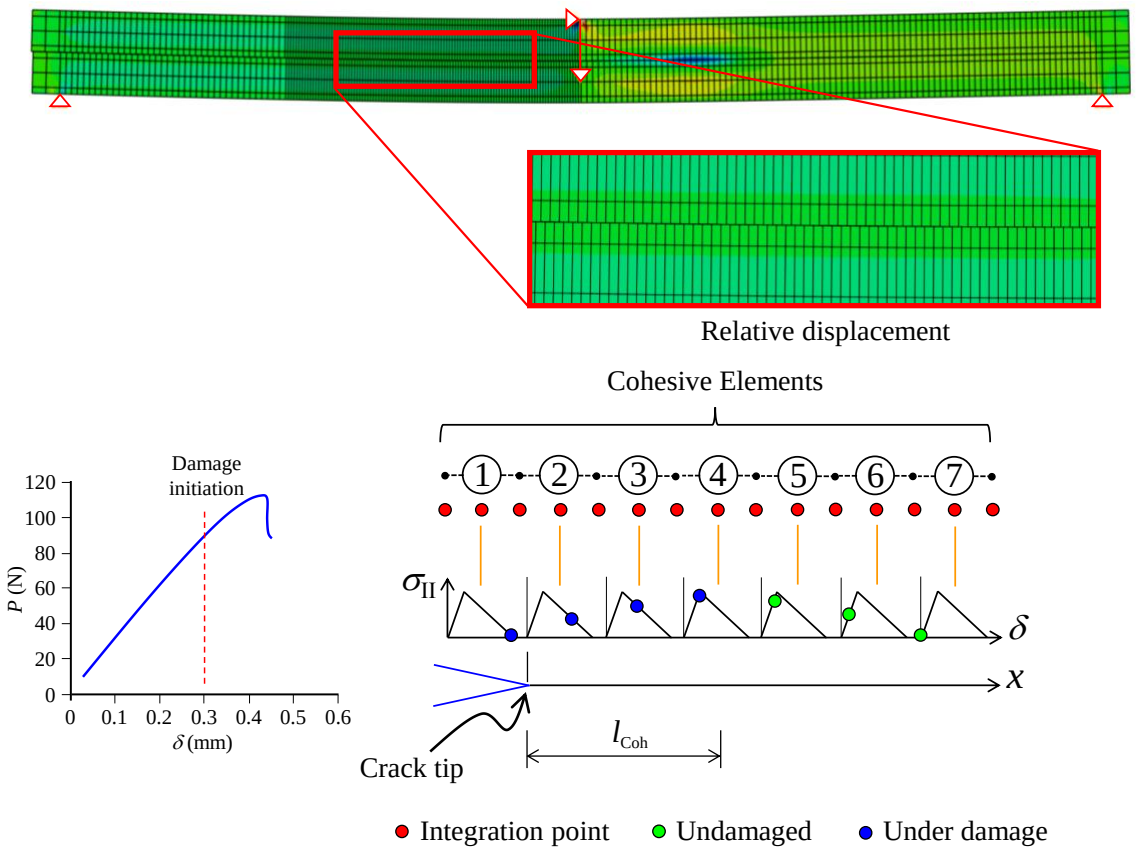

Fig. 8 Cohesive Zone development in mode II loading.

Plots of load-displacement quantities were made from the used data acquisition system (10 Hz), following fracture tests (Figure 10). The obtained curves demonstrate the formation of a non-linear domain prior to the attainment of the ultimate load in different extents (more visible in the first two specimens).

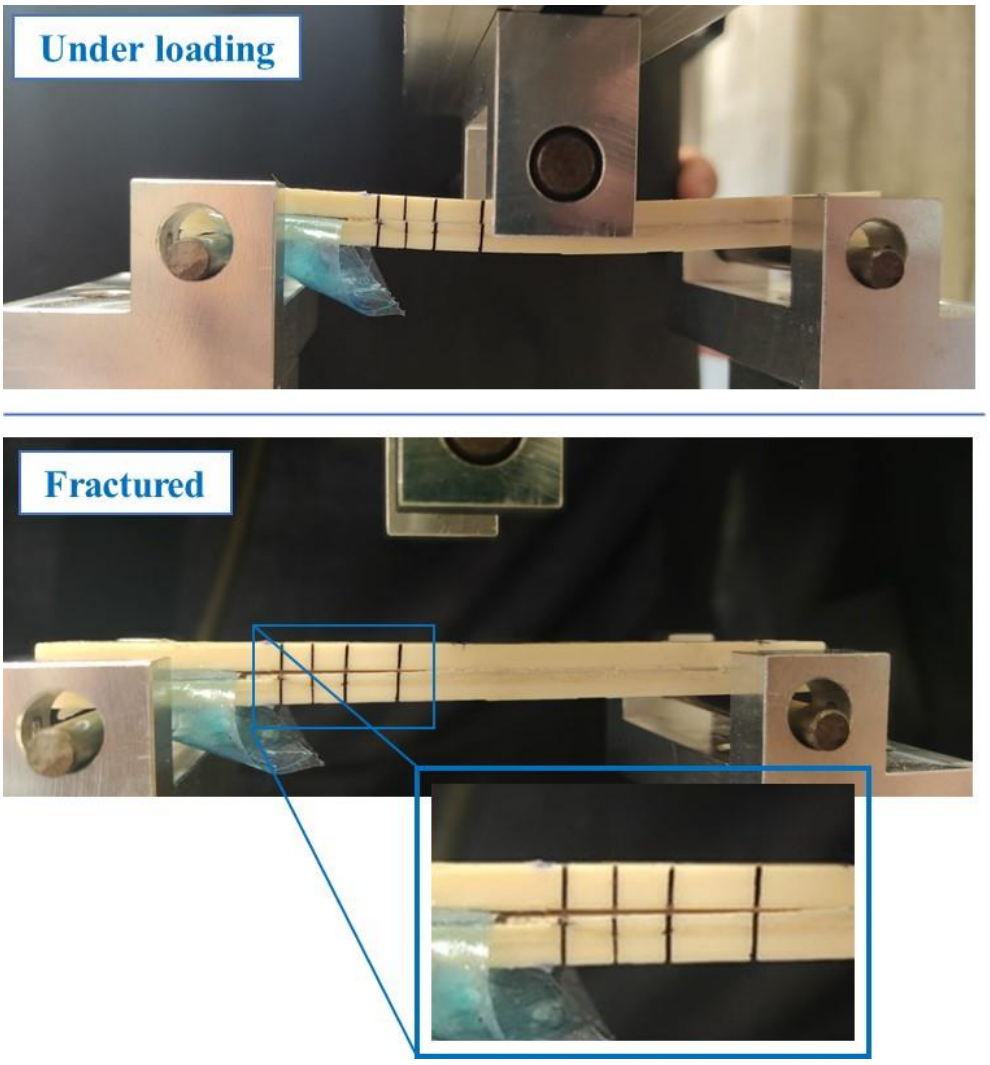

Fig. 9 Condition of a specimen during the ENF test.

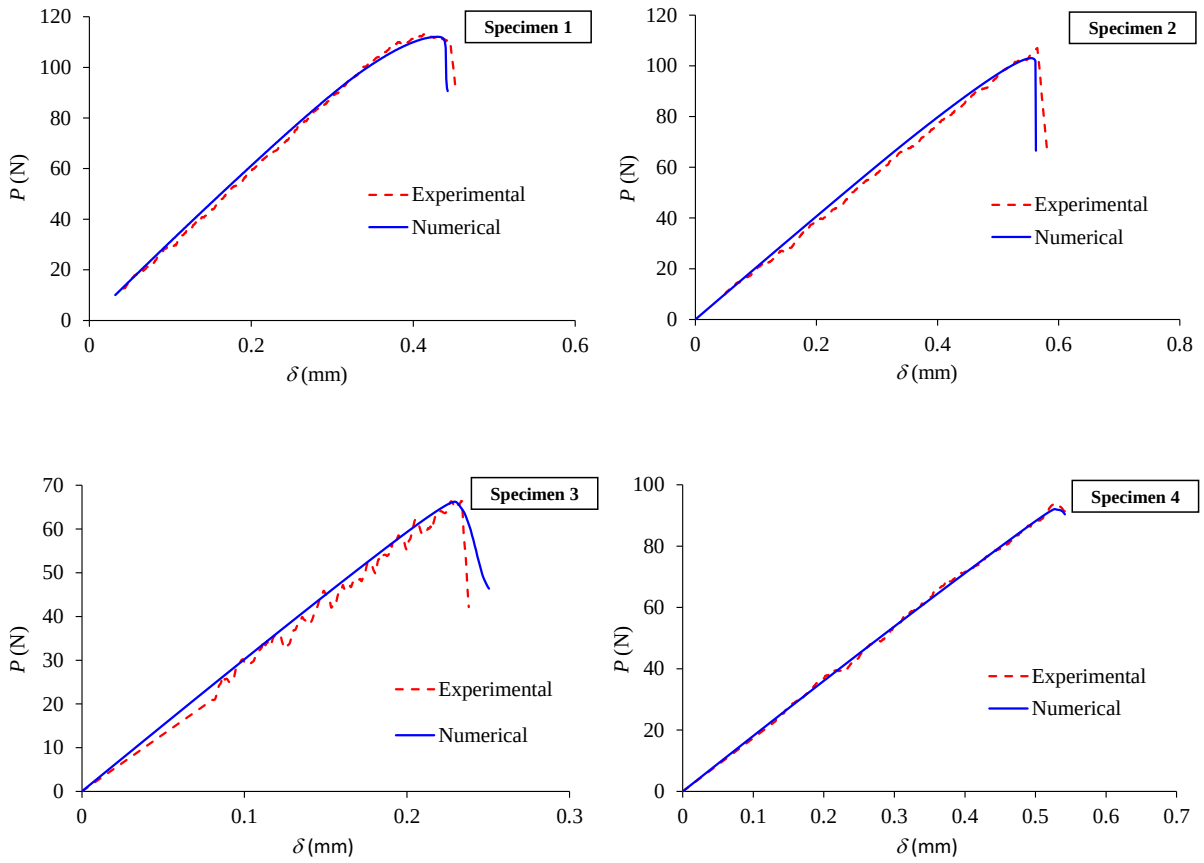

Fig. 10 Load-displacement curves obtained in the ENF test.

Load-displacement curves were used as input to evaluate *R*-curves by means of the CBBM (section 3). This method allows overcoming the difficulties associated with crack monitoring during the ENF test since the crack grows with the specimen parts in close contact with each other. From those curves (Fig. 11), horizontal asymptotes were registered to obtain the critical strain energy release rate G_{IIc} (Table 3), revealing an average value of 0.062 N/mm. This experimental data (i.e., the G_{IIc} values) was then used as input in the inverse method (section 5.1) to identify the cohesive law under pure mode II loading (Fig. 7). This procedure allowed to obtain the numerical agreement shown in Fig. 10 for each specimen, as well as in Fig. 11 for the corresponding *R*-curves (using the numerical *P*-δ curve as input in the CBBM).

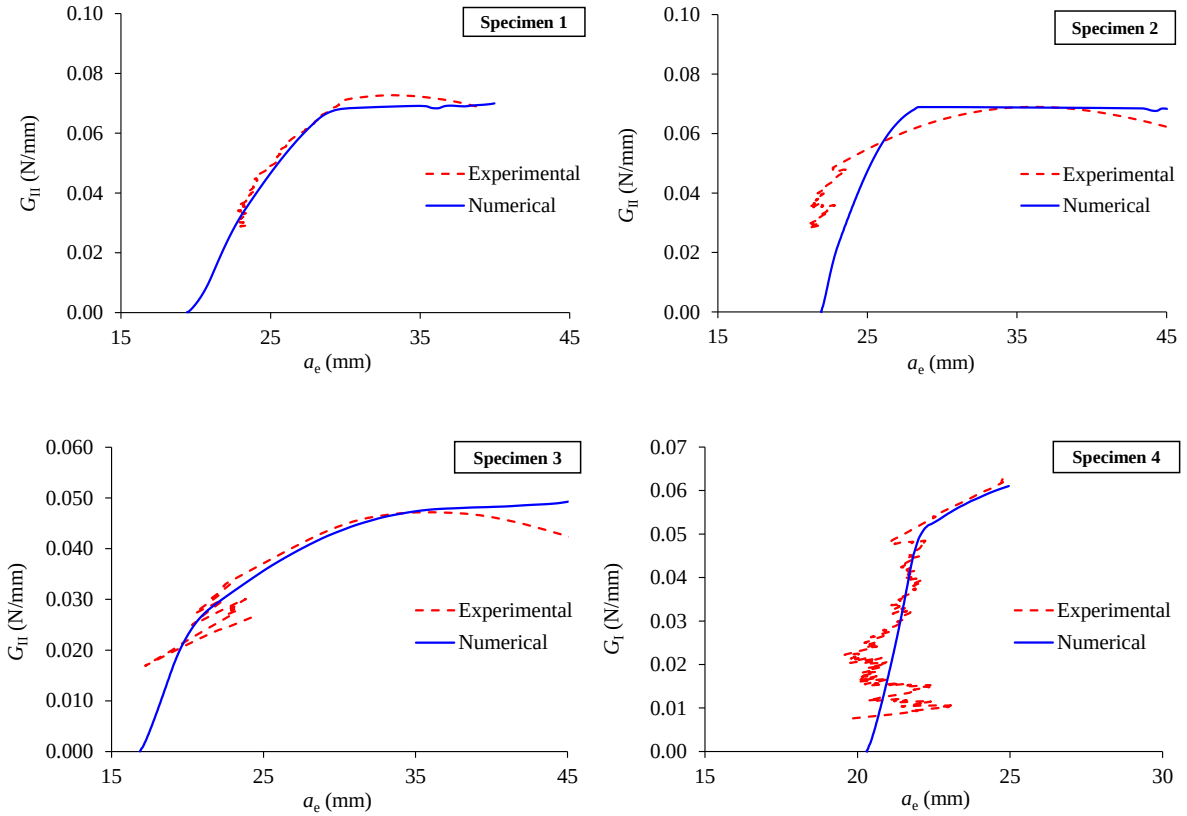

Fig. 11 Numerical-experimental agreement of *R*-curve for mode II loading.

Table 3 Parameters ensued from mode II cement-bone bonded joints

Specimen	G_{IIc} (N/mm)	$\sigma_{II,1}$ (MPa)
1	0.072	3.8
2	0.067	5.5
3	0.050	3.2
4	0.060	4.8
Average	0.062	4.7
CoV (%)	13.3	20.5

As mentioned in section 5.2, the value of critical strain energy release rate G_{IIc} should be analysed simultaneously with the trend of the cohesive zone length l_{coh}. To this aim, plots of such length were made in Fig. 12 as a function of the equivalent crack length (a_e) for each specimen. Strain energy release rate under mode II loading (G_{II}) normalized by the corresponding fracture toughness obtained experimentally (Table 3), i.e., G_{II}/G_{IIc} has also been plotted in the same figure. Both functions were represented using the cohesive laws identified

in the inverse method (section 5.1) for each specimen, which include the value of G_{IIc} (Table 3). These results not only show that the used value of G_{IIc} is well captured by the developed inverse method (i.e., $G_{II}/G_{IIc}=1$ in Fig. 12), but also that the cohesive zone length l_{coh} attained a clear plateau over a significant crack growth extent a_e. It was also verified that the onset of the plateau on the l_{coh} coincide with the attainment of a constant value for the ratio G_{II}/G_{IIc}, which unequivocally proves the fulfilment of the self-similar crack growth for all test specimens in a considerable extent. Another aspect that is worthwhile noting regards the increase in the strain energy release rate (G_{II}/G_{IIc}) with the reduction of the cohesive zone length (l_{coh}) following the plateaus. This behaviour proves that the developed methodology is able to identify limits of toughness measurements for the ENF test, which is an aspect often neglected.

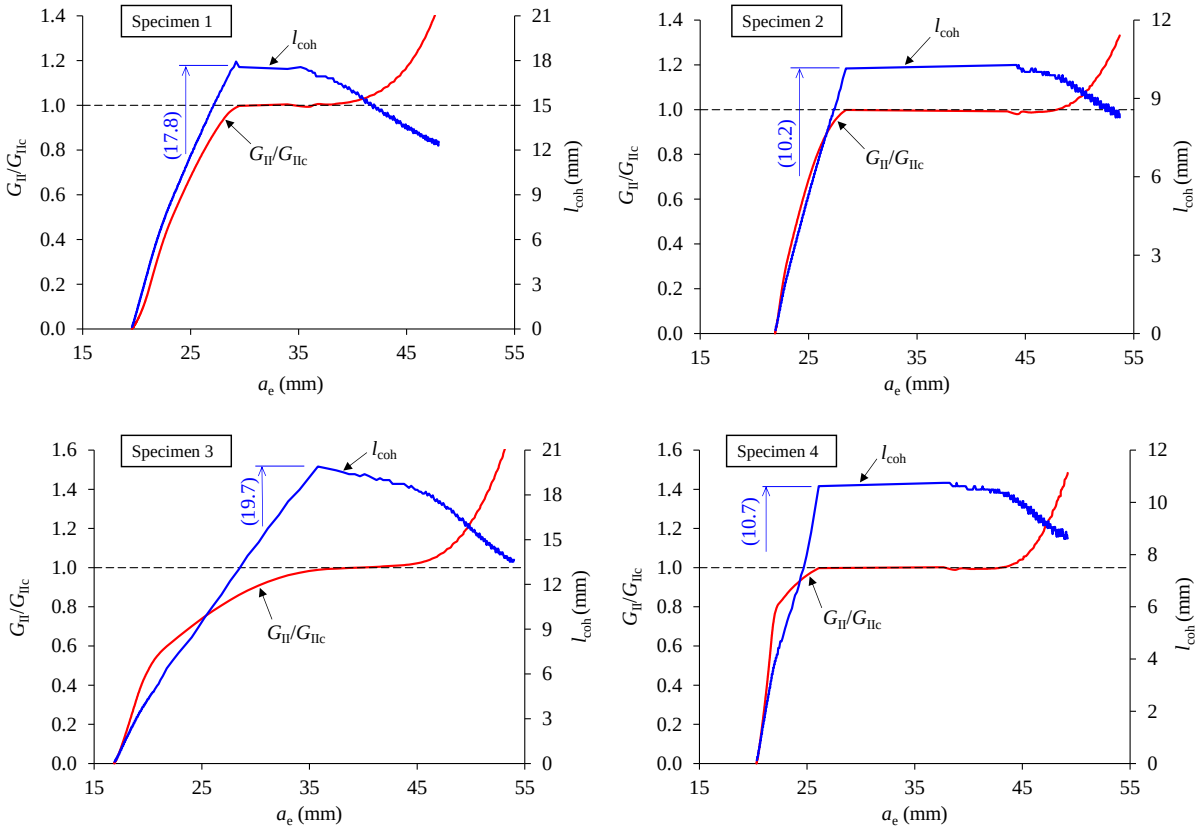

Fig. 12 Evolution of the cohesive length (l_{coh}) and normalized strain energy release rate with the equivalent crack length (a_e).

Figure 13 allows perceiving the evolution of the attained stress (normal and shear components) in the integration points of the cohesive elements (mid-height of the specimen in Fig. 8) disposed along the crack path (*x*-coordinate origin according to Fig. 3) in the increment of crack initiation (from a_0). The inscription a_{num} in Fig. 13 denotes the actual position of the crack tip following the referred propagation increment. Hence, one can note that crack growth has already occurred under pure mode II loading ($\sigma_{II} \neq 0$), since the normal stress has been found negligible at the shear stress peak (i.e., $\sigma_I = 0$). It is also worthwhile noting that for each specimen the shear stress profile (σ_{II}) at the crack tip ($a_{num} \geq a_0$) is fully developed in the domain forming the crack ligament (i.e., $a_0 \leq a_{num} \leq L$) (see Fig. 3) prior to first crack propagation. This means that the developed cohesive zone length (l_{coh}) has not been affected by the loading actuator ($x = L$ in Fig. 13) earlier before the crack propagation had first occurred. Effectively, for each specimen the measure presented in Fig. 13 (i.e., 18.7, 16.2, 24.5 and 13.7 mm) is higher than the one shown in parenthesis in Fig. 12 (i.e., the maximum value of l_{coh}).

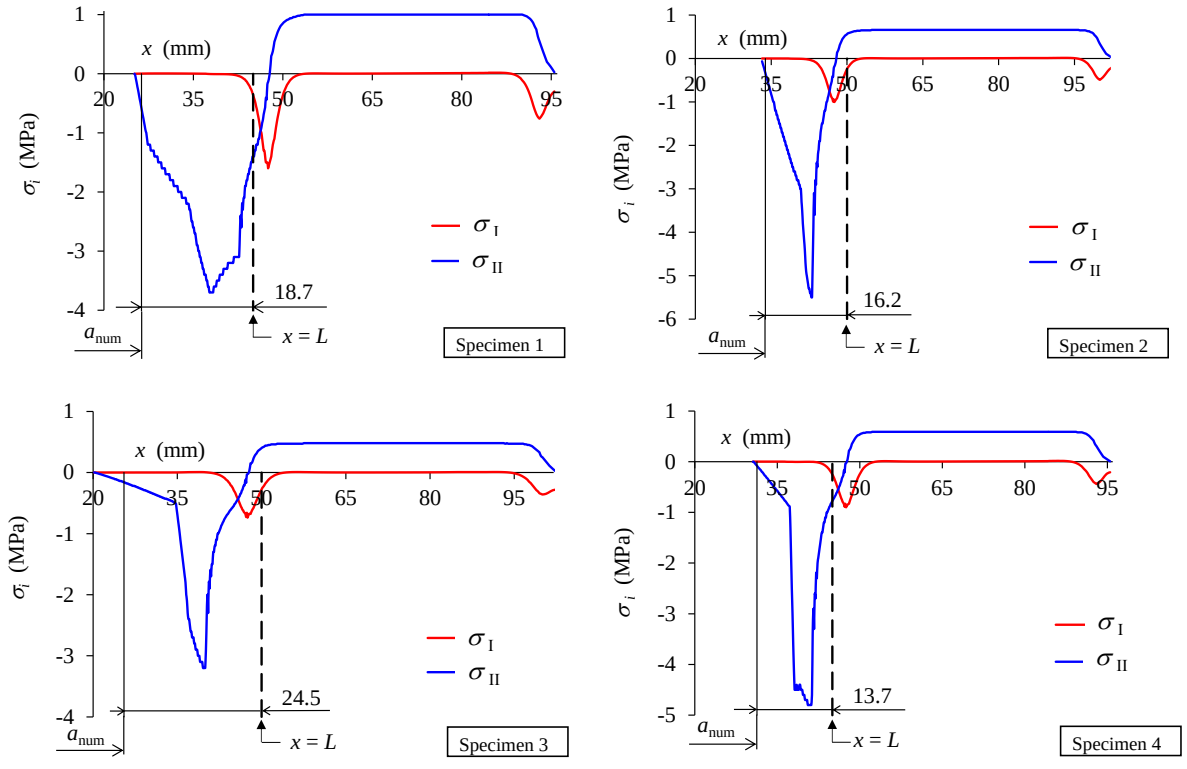

Fig. 13 Normal and shear stress profiles ahead of the crack tip in the increment of crack initiation ($a_{num} \geq a_0$: crack tip position; dashed line denotes the position of the actuator).

The results obtained in this study were also compared with the ones measured by other authors in bone-cement joints with regard to the attained critical strain energy release rate. Hence, Chiang and Hung [15] conducted a set of three-point bending tests (SENB) to evaluate the interfacial fracture toughness of biomaterial composite specimens. The authors used the finite element method, modelling the bovine cortical bone tissue and acrylic bone cement (PMMA) as linear isotropic materials. The fracture energy release rate determined in their work was 0.051±0.058 N/mm. In another study, Lucksanasombool et al. [16] applied the four-point bend interfacial delamination test (4-FPB) to quantify the bonding ability of cements. The authors analysed four conventional bone cements. However, they only obtained results for the glass ionomer cement (FUJI II) and the high viscosity conventional glass ionomer cement (FUJI IX). The calculated strain energy release rate of the FUJI II and FUJI IX groups was 0.053 ±0.085 and 0.044±0.12 N/mm, respectively. Therefore, the average value of the critical energy release rate (G_{IIc}) determined in this study using the CBBM (Table 3) and the ENF test is within the same order of magnitude as the one found in by literature (Fig. 14).

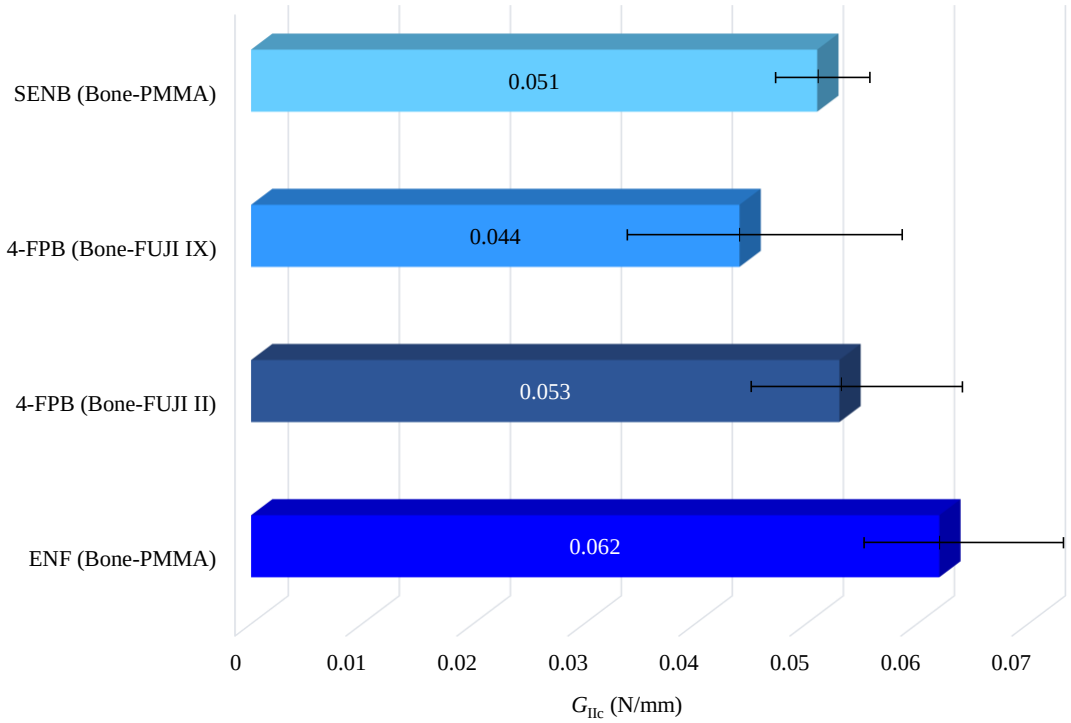

Fig. 14 Values of G_{IIc} obtained by the SENB test [15], the 4-FPB tests [16] and by the ENF test (in this study).

7. Conclusions

This work addresses the evaluation of strain energy release rate of cement-bone bonded joints submitted to mode II loading using the end-notched flexure (ENF) test. Polymethylmethacrylate (PMMA) bone cement was chosen as bonding agent because it is a solution frequently used in the fixation of shoulder and knee prostheses by many surgeons around the world. The strain energy release rate was determined from the *Resistance*-curve evaluated by means of the compliance-based beam method (CBBM) because it does not require monitoring the crack length during the loading process, which is not feasible for the used mechanical test. An inverse method was adopted to estimate the cohesive law characteristic of pure shear loading, which combines numerical and experimental data ensuing from the fracture tests. Based on the attained numerical agreement over the load-displacement curves, plots of the extension of the cohesive zone ahead of the crack tip rendered possible to unequivocally

prove that the development of the fracture process zone is not affected by the actuator (compressive region). This process revealed that the dimensions of the specimens were adequate to accurately estimate the strain energy release rate in the tested cement-bone bonded joints. The obtained value of the strain energy release rate for PMMA bone cement is close to the one estimated by other authors using different test protocols.

Ethical approval: Not required.

Author contribution:

T.D. Campos: Methodology, Investigation, Writing – original draft. **M.L.S. Barbosa:** Investigation, Writing – original draft. **M. Martins:** Software, Resources. F.A. M. Pereira: Methodology, Software, Data curation. **M.F.S.F. de Moura:** Conceptualisation, Methodology, Validation, Software, Writing – review & editing, Supervision. **Quyền Nguyễn:** Software, Resources and Data Curation. **A. Zille:** Conceptualisation, Methodology. **N. Dourado:** Conceptualisation, Methodology, Validation, Writing – review & editing, Supervision, Funding acquisition.

Acknowledgements

The first author acknowledges the Portuguese Foundation for Science and Technology (FCT) for the conceded financial support through the reference grant PTDC/EME-SIS/28225/2017. M.F.S.M. de Moura acknowledges the 'Laboratório Associado de Energia, Transportes e Aeronáutica' (LAETA) for the financial support by the project UID/EMS/50022/2020. The corresponding author also acknowledges FCT for the conceded financial support through the reference projects PTDC/EME-SIS/28225/2017 and UID/EEA/04436/2019.

Competing interests: None declared.

Funding: Portuguese Foundation for Science and Technology for MsC grant of the first author, and research project PTDC/EME-SIS/28225/2017.

1. References

[1] Dourado, N., Pereira, F.A.M., de Moura, M.F.S.F., Morais, J.J.L., Dias, M.I.R. (2013). Bone fracture characterization using the ENF test. Mater Sci Eng. 33:405-410.

[2] de Moura, M. F. S. F., Dourado, N., Morais, J., Pereira, F. A. M. (2011). Numerical analysis of the ENF and ELS tests applied to mode II fracture characterization of cortical bone tissue. Fatigue Fract Eng M. 34:149-158.

[3] Starr, A. J. (2008). Fracture repair: successful advances, persistent problems, and the psychological burden of trauma. J Bone Joint Surg Am, 90, Suppl 1:132-137.

[4] Khaled, S. M. Z., Charpentierand, P.A., Rizkalla, A.S. (2011). Physical and Mechanical Properties of PMMA Bone Cement Reinforced with Nano-sized Titania Fibers. J Biomater. Appl. 25:517-537.

[5] Vaishya, R., Chauhan, M., Vaish, A. (2013). Bone cement, J. Clin Orthop Trauma, 4, Suppl 4:157-163.

[6] Saha, S., Pal, S. (1984). Mechanical properties of bone cement: a review. J Biomed Mater Res, 18, Suppl 4:435-462.

[7] Frias, C., Frazão, O., Tavares, S., Vieira, A., Marques, A.T., Simões, J. (2009). Mechanical characterization of bone cement using fiber Bragg grating sensors. Mater Design. 30:1841-1844.

[8] Jasty, M., Maloney, W.J., Bragdon, C.R., O'Connor, D.O., Haire, T., Harris, W.H. (1991). The initiation of failure in cemented femoral components of hip arthroplasties. J Bone Joint Surg Br. 73:551-8

[9] Sih, G., Bernam, A. (1980). Fracture toughness concept applied to methyl methacrylate. J Biomed Mater Res. 14:311-324.

[10] Lewis, G. (1997) Properties of acrylic bone cements: state-of-the-art-review. J Biomed Mater Res (Appl Biomater) 38:155-18.

[11] Mann, K. A., Mocarski, R., Damron, L. A., Allen, M. J., Ayers, D. C. (2001). Mixed-mode

failure response of the cement-bone interface. J Orthop Res. 19:1153-1161.

[12] Mann, K. A., Bhashyam, S. (1999). Mixed-mode fracture toughness of the cobalt-chromium alloy/polymethylmethacrylate cement interface. J Orthop Res. 17:321-328.

[13] Pereira, F. A. M., de Moura, M. F. S. F., Dourado, N., Morais, J. J. L., Xavier, J., Dias, M. I. R. (2017). Direct and inverse methods applied to the determination of mode I cohesive law of bovine cortical bone using the DCB test. Int. J. Solids Struct. 128:210-220.

[14] Pereira, F. A. M., de Moura, M. F. S. F., Dourado, N., Morais, J. J. L., Silva, F. G. A., Dias, M. I. R. (2016). Bone fracture characterization under mixed-mode I + II loading using the MMB test. Eng. Fract. Mech. 166:151-163.

[15] Chiang, F., Hung, J. (2010).Investigation of the fracture characteristics of the interfacial bond between bone and cement: experimental and finite element approaches. J. Mech. Sci., 24, Suppl 6:1235-1244.

[16] Lucksanasombool, P. , Higgs, W.A.J., Higgs, R.J.E.D., Swain, M.V. (2003). Interfacial fracture toughness between bovine cortical bone and cements. Biomaterials, 24, Suppl 7:1159-1166.